MEASUREMENT AND MODELING OF INTERFERNCE FOR MULTIPLE ANTENNA SYSTEM[1]

Sai Ananthanarayanan P.R., Member, *IEEE*, Alyssa Magleby Richards, Member, *IEEE*, Cynthia Furse, Fellow, *IEEE*

1.1 Abstract

This paper provides a detailed signal model based on network theory to predict the multi-antenna capacity in the presence of co- and adjacent channel interference. This model expands on previous channel models by including the simultaneous effects of interference, antenna matching, efficiency, directivity and polarization. Single and multi-antenna interference are modeled using both a statistical channel model and a site-specific 3D ray tracer. The network theory based detailed signal model was obtained by adding antenna front end effects at both the transmitter and receiver to the channel models. This model was validated with measurements performed in two underground tunnels. The site-specific model predicted the capacity to within 1 bit/sec/Hz of the measurements while the statistical model was within 1-2 bits/sec/Hz except for a few locations. It was also observed that for small antenna spacing the conjugate match provides higher capacity than the self match.

1.2 Introduction

The rapidly growing field of multi-antenna communication contains a great deal of promise for satisfying the future demands of high-speed data transfer across wireless networks. Interference from external sources as well as adjacent users reduces the capacity of the system and must be taken into account. This is particularly true in

[1]Content of this chapter is taken from article co-authored with Alyssa Magleby Richards and Dr. Cynthia Furse and published in Microwave and Optical technology Letters Volume 52 Issue 9, Pages 2031 - 2037

applications where users are tightly packed (in airplanes, buses, buildings, and crowds), where external noise is significant (in aircraft, near other broadcast centers, in industrial plants, etc.), or where communication is particularly sensitive or critical (hospitals, military applications).

This paper evaluates the accuracy with which the performance of a multi-antenna system can be predicted with and without interference using a site-specific 3D ray-tracing algorithm as well as with a more generalized detailed signal model (DSM). This paper first develops a detailed network theory based interference model and studies the effect of interference on the performance of a multi-antenna system by comparing the model with measurements performed inside two different tunnels at the University of Utah. Interference models have been developed in the past for analyzing multi-antenna systems. Blum [1] provides a basic analysis of interference in flat Rayleigh fading channels with no channel state information (CSI) at the transmitter. Yang [2] analyzes the co-channel interference in a Poisson field of interferers. He also analyzes the time dependent correlation of these interfering signals based on the second order statistics of the interference. Song [3] studies the effect of spatially white and colored interference and noise with fixed total interference plus noise power. The analysis in [3] using different CSI at the transmitter and receiver has shown that the capacity is higher for the case where there are fewer high-data rate interferers. Koivunen [4] studies the effects of interference on a dynamic multi-link wideband MIMO channel indoor measurement campaign at 5.3 GHz and shows a strong correlation between the relative capacity and signal to interference ratio (SIR). All these interference models although provide approximations do not include the effects of RF front end at the transmitter and receiver

that has been shown by Landon [5] to affect the system performance. This paper provides a detailed interference analysis extending Landon's transmission equation model [5] and studies the effect of each individual parameter on the estimated capacity. The model uses a 3D ray-tracing site specific channel model or a more generalized detailed signal model and these results are compared to measurements in the two tunnels. The detailed signal model includes the effects of model which includes the effect of antenna polarization misalignment, correlation, mutual coupling, and radiation efficiency which have been found to have an effect on the system performance. [5]

Section 5.3 briefly describes the detailed signal model for multi-antenna systems developed by Landon [5] for indoor wireless communication and the 3D ray-tracing model [6] which was adapted to the tunnel environment. The ray-tracing software initially developed for stairways and indoor environments [6] are changed to the shape and size of the Merrill Engineering building (MEB) and the Park building tunnel at the University of Utah which were used for performing measurements. Section 5.4 expands the detailed signal model to include the effects of interference and compares it with other well known interference models for multi-antenna systems. Section 5.5 describes the measurement setup and the measurement process used for obtaining the channel matrix ***'H'*** in both the tunnels.

Section 5.6 compares the capacity obtained using the measurements in the tunnels with a 4 x 4 multi-antenna system to those predicted using the 3D ray-tracing model and the detailed signal model with and without interference. Both the ray-tracing based model as well as the detailed signal model were studied to see if these models could approximate the system performance or whether rigorous measurement campaigns need

UU IR Author Manuscript

to be undertaken. In this section we also compare the effects of self and conjugate matching on varying antenna spacing for a simple 2 X 2 multi-antenna system in the presence of co-channel interference.. The study of various matching techniques helps us to determine which matching technique would provide good performance for multi-antenna system with varying spacing.

1.3 Channel Models

This section describes the channel models that we will use to analyze multi-antenna systems. The channels include the ray-tracing channel model and the detailed signal model.

1.3.1 Detailed Signal Model

Figure 5.1 shows the MIMO system model relating transmit input voltages, [x_1 ... x_M], to receive voltages [y_1 ... y_N] as a function of channel and system design parameters. M_R is the N x N impedance matrix describing the receive antenna array, E_{cdr} is the diagonal matrix containing the radiation (conduction and dielectric) efficiencies, $e_{cdr,i}$ of the N receive antennas. D_R and P are diagonal matrices of distributed directivities and system polarization alignments, and R_s is the spatial correlation of the signals impinging on the receiver—traditionally including the effects expressed in D_R and P, but broken out separately in our model. Corresponding matrices for the transmit array are denoted by a subscript T or t. Grouping designators are also included for later reference: H_{LMU} represents a lossless, matched, uncoupled channel matrix, H_{DP} adds directivity and polarization alignment effects, and H represents a complete system channel matrix.

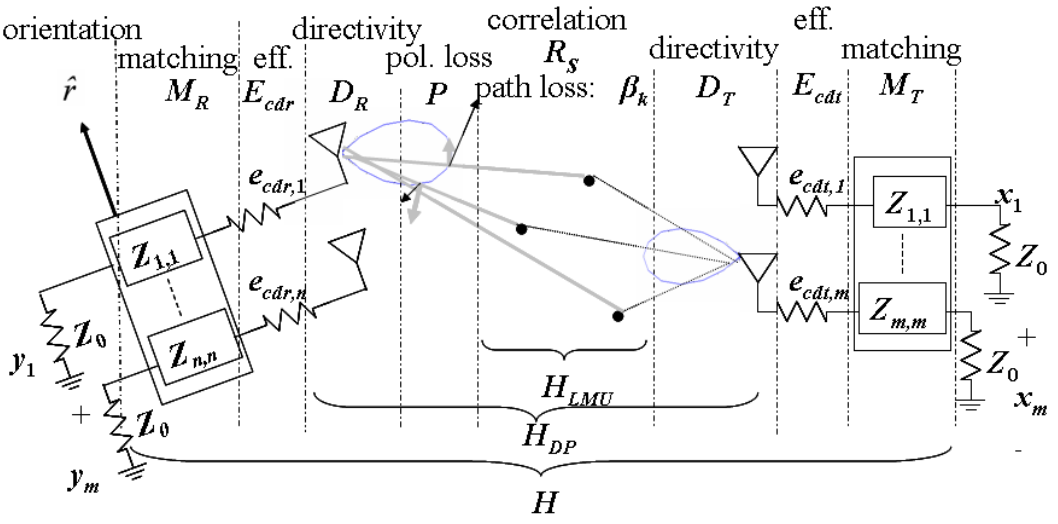

Figure **Error! No text of specified style in document.**.1: A general MIMO system model

The receive antenna voltages can be expressed as:

$$y = \underbrace{\underbrace{Z_0^{1/2}\underbrace{S_{21}}_{\text{matching}}(\mathbf{I}-\mathbf{S}_{RR}S_{11})^{-1}\left(\mathbf{I}+\frac{\mathbf{Z}_{RR}}{Z_0}\right)^{-1}\underbrace{\mathbf{E}_{cdr}}_{\substack{\text{rad}\\ \text{eff}}}}_{M_R}\left[\frac{1}{Z_0}\sum_{k=1}^{N_p}\underbrace{E_i^R(AOA_k,\hat{r})}_{\text{directivity}}\cdot\underbrace{\hat{p}_T}_{\text{pol. loss}}\underbrace{\beta_k}_{\text{path loss}}\underbrace{e_j^T(AOD_k)}_{\text{directivity}}\right]}_{H_{DP}}\underbrace{\mathbf{E}_{\mathbf{cdt}}}_{\substack{\text{rad}\\ \text{eff}}}\underbrace{(\mathbf{I}-\mathbf{S}_{TT})}_{\text{matching}}}_{M_T}}_{H} x, \tag{5.1}$$

This method uses gain pattern, for the i^{th} receive antenna, $E_i^R(AOA)$, and trans-impedance gain pattern for the j^{th} transmit antenna, $e_j^T(AOD)$, as a function of angle-of-arrival (*AOA*) and -departure (*AOD*) to determine the effective signal y and hence capacity C_E within the model. Z_0 is the characteristic impedance, $\boldsymbol{S}_{TT}$ and $\boldsymbol{S}_{RR}$ are the scattering parameters of the unloaded transmit and receive arrays respectively, $\boldsymbol{S}_{RT}$ is the channel scattering matrix, and S_{11} and S_{21} represent a matching circuit and transmission circuit for a selected matching approach. Receive and transmit antenna efficiencies, $\boldsymbol{E}_{cdr}$ and $\boldsymbol{E}_{cdt}$, are also included. The effect of receive array orientation, $\hat{r}$, is included through the gain term $E_i^R(AOA,\hat{r})$. The polarization loss is the dot product between the gain term $E_i^R(AOA,\hat{r})$ and the unit vector describing the polarization of the impinging signal, $\hat{p}_T$.

UU IR Author Manuscript

The influence of the channel on channel-system capacity is expressed as a summation of N_p plane waves where the k^{th} plane wave has complex gain (path loss and phase shifts) β_k.

Including the Ricean K factor which is found from the single antenna measurements, the channel matrix $\boldsymbol{H}$ can be written as [12]:

$$H = \sqrt{\frac{K}{K+1}}\mathbf{H}_{ricean} + \sqrt{\frac{1}{1+K}}\mathbf{H} \quad (2)$$

where K is the Ricean K-factor obtained from [13].

1.3.2 3D Ray-tracing Model

A site specific 3D ray-tracing model [7] was used for analyzing the channel in the tunnel for both signal and interference analysis. [8] The model uses the triangular grid method to determine which rays arrive at the receive antenna. The algorithm uses 30% or less CPU time than traditional ray-tracing methods and has been validated in 2D environments for indoor and outdoor multipath environments, and in a 3D environment for reflections in stairwells. [7][9] The software was adapted to a multi-antenna system by running the ray tracer multiple times for different antenna locations rather than just a single set at a time. The tunnels were modeled with 12 rectangular facets to represent the floor, ceiling, walls, and ramp. Figure 2 shows the model for MEB tunnel. The MEB tunnel is a small underground tunnel with dimension of 2.64 m X 5.51m X 20m. The walls and the floor were modeled as cement structures with permittivity (ε_r) of 8.1 F/m and conductivity of 0.0352 S/m (obtained from measurements using dielectric probes). The maximum number of projected rays is 320 which is attained when 15 or more bounces are allowed before a ray reaches the receiver. Figure 3 shows the model for the Park building tunnel which was modeled as a concrete structure with a permittivity (ε_r) of

5.1 F/m and conductivity of 0.000152 S/m. The Park building tunnel is a wider and longer tunnel with dimensions 4.572m X 3.66m X 50m. The 3D ray-tracing software provides the complex electric fields and angle of arrival and departure for each antenna pair. These parameters were used for obtaining the channel matrix '*H'* which is given as:

$$\mathbf{H} = \underbrace{Z_0^{1/2} \underbrace{\mathbf{S}_{21}(\mathbf{I}-\mathbf{S}_{RR}\mathbf{S}_{11})^{-1}}_{matching} \left(\mathbf{I}+\frac{\mathbf{Z}_{RR}}{Z_0}\right)^{-1} \underbrace{\mathbf{E}_{cdr}}_{rad\ eff}}_{M_R} H_{3D} \underbrace{\mathbf{E}_{cdt}}_{rad\ eff} \underbrace{(\mathbf{I}-\mathbf{S}_{TT})}_{matching}, \tag{5.3}$$

The capacity for both these channels can be estimated as:

$$C = \log_2 \det[\mathbf{I} + \frac{SNR_r N_r}{\| \mathbf{H} \|^2_{Frobenius}} \mathbf{H}\mathbf{H}^H] \tag{5.4}$$

The two channel models described in this section will be used for performing interference analysis, and the resultant capacities will be validated by comparing them to the measured capacities in section V.

1.4 Interference Model

Blum's analysis of multi-antenna system capacity with interference [1] considers a Rayleigh fading channel with no CSI at the transmitter. It provides the system capacity for a single user with multiple transmit and receive antennas. Extending it to *L* users in the system where the *L-1* users' act as interferers, the received signal can be written as:

$$r_L = \sqrt{\rho_L} H_{L,L} x_L + \sum_{J=1}^{L-1} \sqrt{INR_{L,j}} H_{L,j} x_j \tag{5.5}$$

where $H_{L,j}$ and x_j represent the normalized channel matrix elements and normalized transmitted signal of user *j*, respectively. The noise vector and channel matrix are assumed to have independent and ideally distributed zero mean and unit variance

complex Gaussian entries. ρ_L is the SNR of user L, and $INR_{L,j}$ is the INR for user L. The mutual information is then given by

$$I(x_L;(y_L,H)) = E\{\log_2[\det(\mathbf{I}_{n_r} + \rho_i \mathbf{H}_{i,i}\mathbf{Q}_i\mathbf{H}_{i,i}^H(\mathbf{I}_{n_r} + \sum_{j=1,j\neq i}^{L} INR_{i,j}\mathbf{H}_{i,j}\mathbf{Q}_j\mathbf{H}_{i,j}^H)^{-1}]\} \quad (5.6)$$

where $E\{\}$ stands for expectation and $\mathbf{Q}$ is the covariance matrix of the transmitted signal.

Song [2] considers the effect of spatially white and colored interference and noise with fixed total interference plus noise power. The mutual information between the channel input and output is given by

$$I(x;y) = \log_2 \det[\mathbf{I}_\mathbf{N} + (\mathbf{R}^{-1/2}\mathbf{H})\frac{\mathbf{Q}}{\sigma^2}(\mathbf{R}^{-1/2}\mathbf{H})^T] \quad (5.7)$$

where R is given as

$$R = \frac{INR}{L}\sum_{i=1}^{L} h_i h_i^T + I_N \quad (5.8)$$

If transmit power is constrained such that $trace\ (Q) < P_T$, where P_T is the transmit power and $\boldsymbol{H}$ is the channel matrix, the capacity equation can be given by

$$C = \max \log_2 \det[\mathbf{I}_\mathbf{N} + (\mathbf{R}^{-1/2}\mathbf{H})\frac{\mathbf{Q}}{\sigma^2}(\mathbf{R}^{-1/2}\mathbf{H})^T] \quad (5.9)$$

where σ^2 is the noise variance. Applying the interference model developed by Blum [1] and Song [3] to the network theory model [10] we obtain the mutual information expression as

$$I(y_L,x_L) = \log_2 \frac{|\mathbf{P}_N\mathbf{S}_{RT}\mathbf{Q}\mathbf{S}_{RT}^H\mathbf{P}_N^H + \mathbf{P}_N\mathbf{K}_N\mathbf{P}_N^H|}{|\mathbf{P}_N\mathbf{K}_N\mathbf{P}_N^H|} \quad (5.10)$$

where

UU IR Author Manuscript

$$\mathbf{P}_N = S_{21}(I - \mathbf{S}_{RR}S_{11})^{-1} \tag{5.11}$$

and K_N is $E\{n_1\ n_1{}^H\}$ where n_1 is the noise vector. For a Gaussian channel with $K_N=\sigma^2\mathbf{I}$ the capacity is

$$\mathbf{I}(y_L, x_L) = \log_2 \frac{|\mathbf{P}_N\mathbf{S}_{RT}\mathbf{Q}\mathbf{S}_{RT}^H\mathbf{P}_N{}^H + \mathbf{P}_N\mathbf{K}_N\mathbf{P}_N{}^H|}{|\mathbf{P}_N\sigma^2\mathbf{P}_N{}^H|} \tag{5.12}$$

If P is non-singular (8) reduces to

$$I(y_L, x_L) = \log_2 |\frac{S_{RT}QS_{RT}^H}{\sigma^2} + I| \tag{5.13}$$

If we assume there are L channels arriving at each receiver the received signal y can be given by:

$$v_R = Z_0{}^{\frac{1}{2}}S_{21}(I - \mathbf{S}_{RR}S_{11})^{-1}[\mathbf{S}_{RT,L}a_{T,L} + \sum_{j=1}^{L-1}\mathbf{S}_{RT,j}a_{T,j}] + Noise \tag{5.14}$$

where $\mathbf{S}_{RT,L}$ is the channel scattering matrix for the L^{th} transmitter and *Noise* is the noise matrix. In this section we assume the noise to be Gaussian with variance σ. The equivalent capacity is given as:

$$I(y_L, x_L) = \log_2 \frac{|\mathbf{S}_{RT,j}\mathbf{Q}_j\mathbf{S}_{RT,j}^H\mathbf{R}^{-1} + Noise|}{|Noise|} \tag{5.15}$$

$$\mathbf{R} = \sum_{j=1}^{L-1}\mathbf{S}_{RT,j}\mathbf{Q}_j\mathbf{S}_{RT,j}^H + \mathbf{I} \tag{5.16}$$

Extending this analysis to the multi-antenna model in (1) with interference we obtain the received signal as:

$$y = Z_o^{1/2} S_{21}(I - \mathbf{S}_{RR} S_{11})^{-1}(\mathbf{I} + \frac{\mathbf{Z}_{RR}}{Z_o})^{-1}\mathbf{E}_{cdr}[[\frac{1}{Z_o}\sum_{k=1}^{N_i} E_i^R(AOA_{k,L}, r)\, p_r \beta_{k,L} e_j^T (AOD)_{k,l}]\mathbf{E}_{cdt,L}(\mathbf{I} - \mathbf{S}_{TT,L})x_L$$
$$+ \sum_{a=1}^{L-1}[\frac{1}{Z_o}\sum_{k=1}^{N_i} E_i^R(AOA_{k,a})\, p_r \beta_{k,a} e_j^T (AOD)_{k,l}]\mathbf{E}_{cdt,a}(\mathbf{I} - \mathbf{S}_{TT,a})x_a \tag{5.17}$$

and the equivalent capacity is given by

$$C_E = E\{\log_2 | I + \mathbf{M}_R \mathbf{E}_{cdr} \mathbf{H}_{DP} \mathbf{E}_{cdt} \mathbf{Q} (\mathbf{M}_R \mathbf{E}_{cdr} \mathbf{H}_{DP} \mathbf{E}_{cdt})^H \mathbf{R}^{-1} \frac{1}{\sigma^2} |\} \tag{5.18a}$$

where

$$R = \mathbf{I} + \sum_{j=1}^{L-1} \mathbf{M}_R \mathbf{E}_{cdr} \mathbf{H}_{DP} \mathbf{E}_{cdt,j} \mathbf{Q}_j (\mathbf{M}_R \mathbf{E}_{cdr} \mathbf{H}_{DP} \mathbf{E}_{cdt,j})^H \tag{5.18b}$$

This expression will be validated in section 5.5 by comparing it with the measured capacities obtained in the tunnels.

1.5 Measurements

Measurements were taken in the two tunnels to validate the capacity expressions in (518a). For the MEB tunnel in figure 5.2 eight transmitter locations were chosen throughout the tunnel and the receiver was placed at the entrance of the tunnel. The transmitters were placed with a separation of 2.23 meters along the width of the tunnel and 2.43 meters along the length of the tunnel. Transmitters Tx1 and Tx2 were closest to the receiver and were placed at a distance 3.53m from it. In the Park building tunnel four transmitter locations were chosen throughout the tunnel and the receiver was placed at the entrance of the tunnel as shown in figure 5.3. The transmitters were placed with a separation of 6 meters along the length of the tunnel and at the center along the width.

UU IR Author Manuscript

Transmitter Tx1 was closest to the receiver and was placed at a distance 6 m from it.

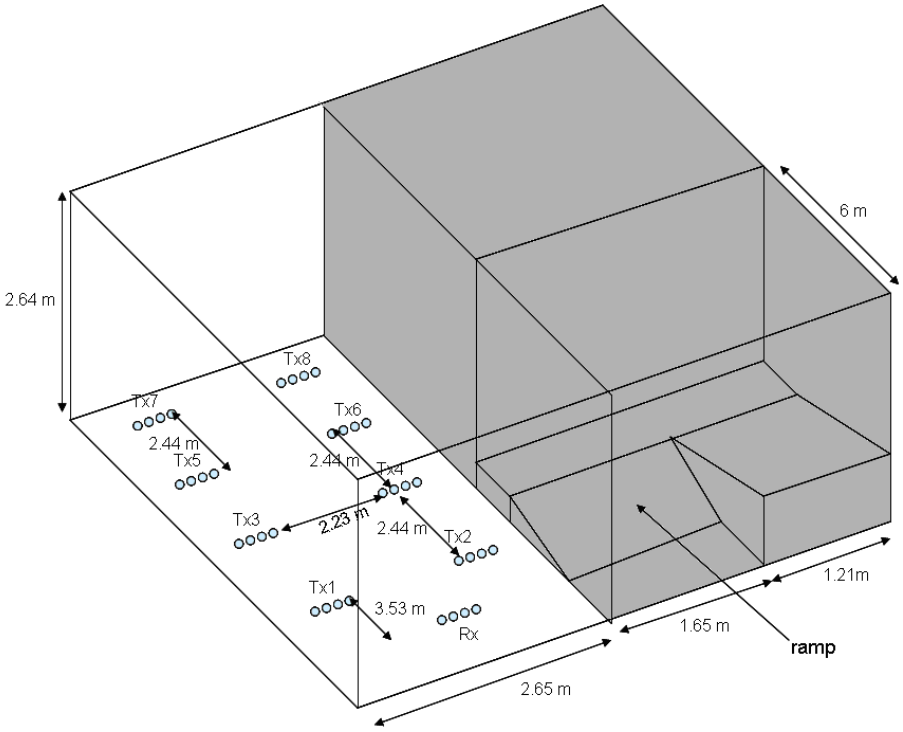

Figure **Error! No text of specified style in document.**.2: MEB Tunnel with dimensions 2.64m X 5.51m X 20m with permittivity (ε_r) of 8.1 F/m and conductivity of 0.0352 S/m

The measurements were taken using the University of Utah multi-antenna testbed which has 4 X 4 multi-antenna systems with dipole antennas separated by 0.25λ [11]. Measurements were taken by broadcasting a training packet of data, and thereby providing a direct measurement of the channel matrix for that given transmitter/receiver pair. The transmit array was then moved to the next location where another packet was transmitted. This cycle was then repeated until the survey of the tunnel was completed. As long as the environment within the tunnel was unchanged over the measurement cycle, all channel matrices may be treated as though they were obtained simultaneously. For the MEB tunnel two single antenna interferers were placed at locations Tx7 and Tx3 as shown in figure 5.2, and the receiver was placed at the same location as in the multi-

antenna case. In the Park Building tunnel the single antenna interferer was placed at location Tx3 as shown in figure 5.3, and the receiver was placed at the entrance of the tunnel as shown in figure 5.2. Single antenna interference was generated by transmitting a continuous wave signal at 915 MHz with varying INR using an Agilent E4438C vector signal generator. The signal was sampled using the receiver MIMO testbed and the channel matrix for the interferers was obtained.

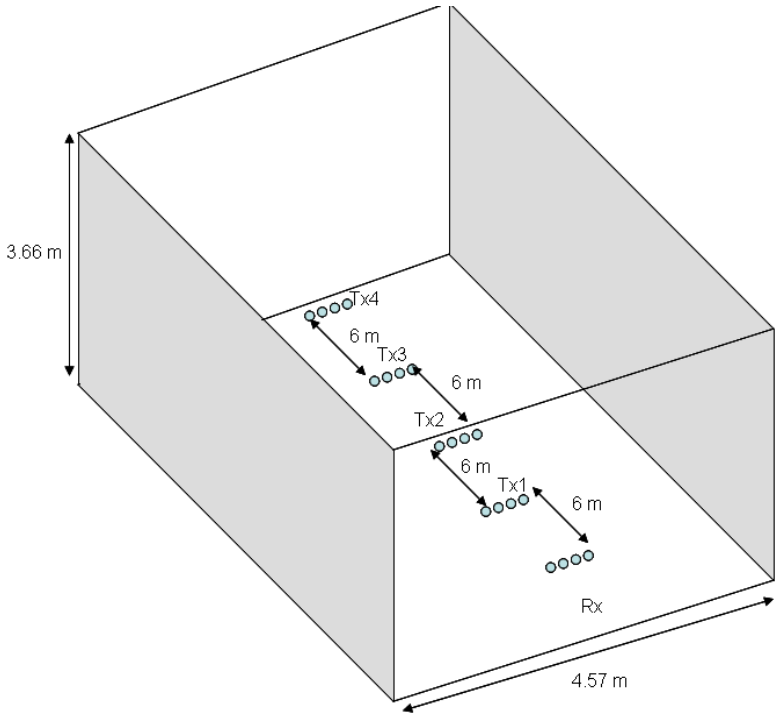

Figure **Error! No text of specified style in document.**.3: Park Tunnel with dimensions 4.572m X 3.66m X 50m and permittivity (ε_r) of 5.1 F/m and conductivity of 0.000152 S/m.

A fortunate aspect of channel capacity measurement is that one need not physically implement a given algorithm in order to calculate its potential capacity. In fact, the only requisite measurement is a set of H-matrices over the various test locations. It is therefore important to understand how a channel matrix is computed from a packet of data. We begin by defining a complex *M* x *W* matrix **T**, called the training sequence,

and write it as a series of column vectors with the form

$$T = [\ t(1)|\ t(2)|\ \_\ \_\ \_\ |t(W)\ ] \tag{5.19}$$

In other words, each column vector t(*w*) represents an M x 1 vector of complex data symbols being broadcast by the transmitter at time . The N x W matrix of sampled symbols at the k^{th} receiver may therefore be written as:

$$Y = \mathbf{HT} + \mathbf{N}_{noise} \tag{5.20}$$

where, **N** is simply an *N* x *W* matrix of sampled noise.

Because **T** is a known sequence of data, it can be used to estimate the channel matrix. Defining the matrix as the channel matrix estimate, we may simply write:

sequence of data, it can be used to estimate the channel matrix as:

$$\tilde{\mathbf{H}} = \mathbf{YT}^{+} = \mathbf{H} + \mathbf{N}_{noise}\mathbf{T}^{+} \tag{5.21}$$

where $\mathbf{T}^{+}$ denotes the Moore-Penrose pseudo inverse of **T**, and is given by

$$\mathbf{T}^{+} = (\mathbf{T}^{H}\mathbf{T})^{-1}\mathbf{T}^{H} \tag{5.22}$$

As long as the SNR at the receiver is relatively large, the effects of the noise term $\mathbf{N}_{noise}$ are negligible, and $\tilde{\mathbf{H}}$ transforms to **H .** The effects of noise may be further reduced by choosing a relatively large value for W. This is because the quantity $\mathbf{N_{noise}T}^{+}$ behaves much like a correlation between the training sequence and the noise. Thus, in the limit as $W \rightarrow \infty$, we have $\mathbf{N_{noise}T}^{+} \rightarrow 0$ for uncorrelated noise. So as long as the channel itself remains stationary over the duration of the training sequence, *W* may be chosen as any arbitrarily large value. For the data presented in this paper, all channel matrices were estimated using a training sequence of pseudorandom data with length W = 4000.

Multi-antenna capacity computed in this section will compare the channel models obtained from measurements, the 3D ray-tracing model as well as the detailed signal

model. To provide consistency of gain between antennas, all sampled data were normalized to a unit noise variance at each antenna. This was accomplished by isolating an unused portion of the spectrum and applying the matched filter as if there were actual data. The resultant noise variance was then used as the normalization factor for the antenna. Also, it is common in MIMO measurements to normalize the channel matrices in order to eliminate capacity variations due to path loss. The resultant capacity after normalization is thus a reflection of the relative multipath richness of the channel, rather than any particular gain due to proximity with the transmitter. For our data, all channel matrices were fixed to a unit Frobenius norm. That is to say, $||H|| = 1$ for all data. Symbol power was then fixed to the arbitrary value of $Ps = 100$, thereby giving an *SNR* of 20 dB.

1.6 Results

In this section we will first validate the 3D ray-tracing and the detailed signal models by comparing the capacities obtained using them to the measurements in the tunnels. After validating the models they will be used for estimating the capacity in the presence of interference in the same tunnel environment. Following this the effects of both conjugate matching and self matching on 2 X 2 MIMO performances for varying antenna spacing will be presented.

UU IR Author Manuscript

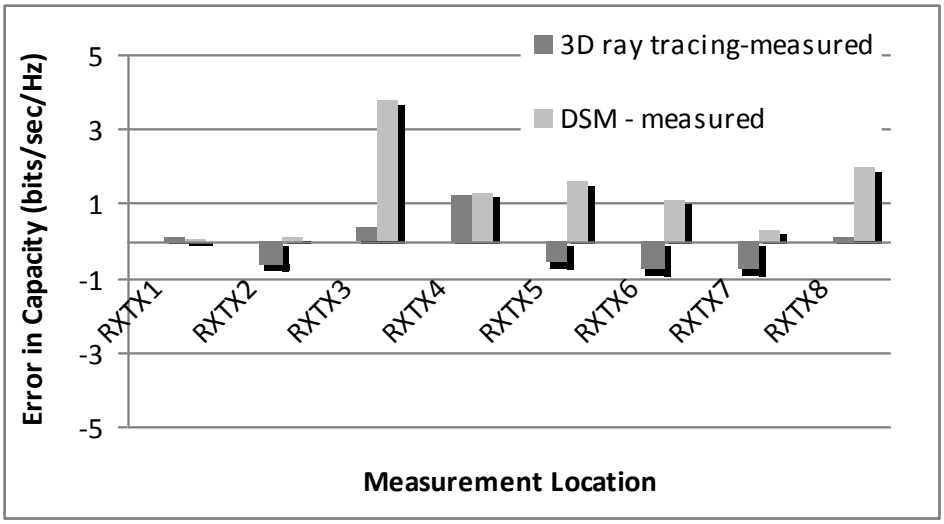

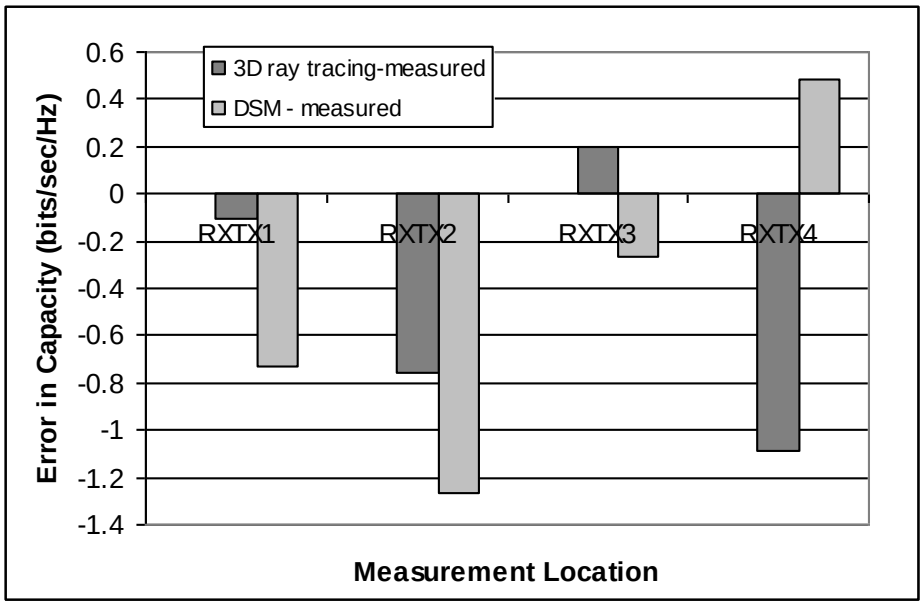

Figure **Error! No text of specified style in document.**.4: Error between the measured and the simulated capacities for the MEB Tunnel and the Park building tunnel

Figure 5.4 shows the error between the measured and the simulated capacities for the tunnels. From figure 5.4 we observe that for both tunnels the 3D ray-tracing algorithm estimated the capacity within 1 bit/sec/Hz. The detailed signal model was equally accurate except for MEB locations Tx3 and Tx8, possibly because of the richness of multipath at these locations. These results show that both the 3D and the detailed signal model (DSM) provide accurate channel matrices and hence capacity for midsize tunnels.

UU IR Author Manuscript

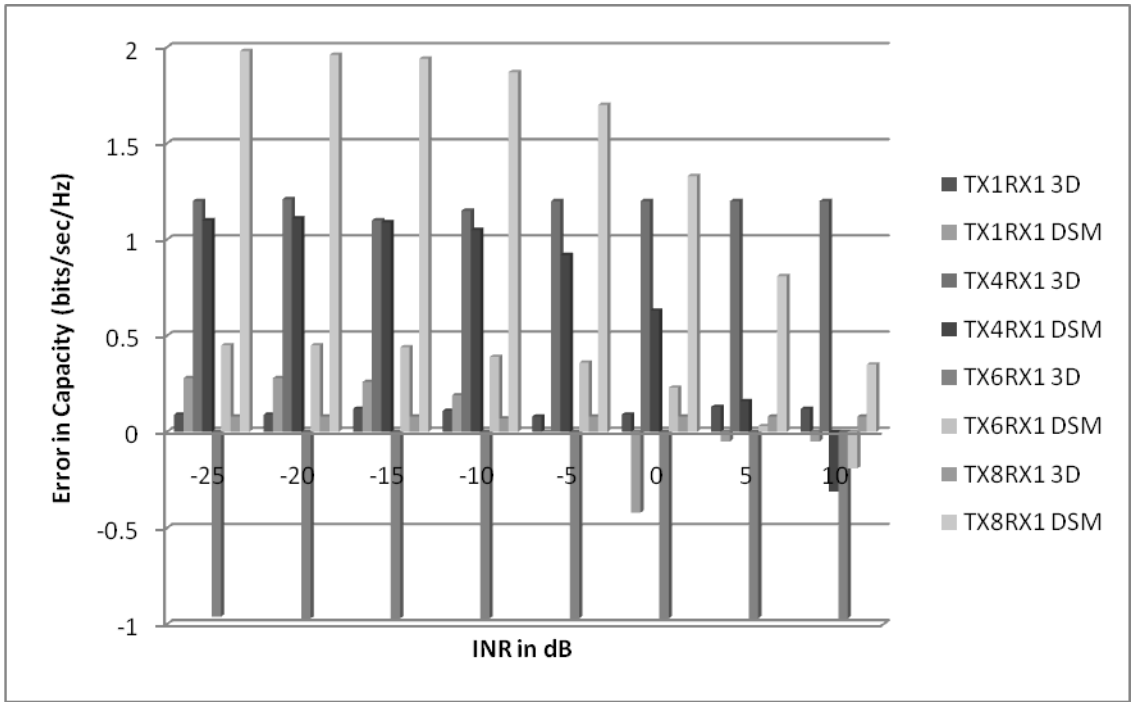

Figure **Error! No text of specified style in document.**.5: MEB Tunnel error in capacities between the measurements and 3D ray-tracing model (3D), and measurements and Detailed signal model (DSM) with single-antenna interferer located at Tx7 in figure 5.1. Four transmitter locations Tx1, Tx4, Tx6 and Tx8 were used for measurements.

Interference measurements were performed in both tunnels as explained in section II. For the MEB tunnel the single and multi-antenna interferers were placed at transmitter locations Tx7 and Tx3 as. For the Park building tunnel the single and multi-antenna interferers were placed at transmitter location Tx3. Figure 5.5 summarizes the error between the measured capacity and the capacity obtained using the 3D ray-tracing and the detailed signal models at the various locations in the MEB tunnel in the presence of single antenna interference. Figure 5.6 summarizes the error in the presence of multi-antenna interference. Figures 5.7 and 5.8 summarize the error between the measured capacity and the capacity obtained using the 3D ray-tracing and the detailed signal model for single and multi-antenna interference in the Park building tunnel respectively.

UU IR Author Manuscript

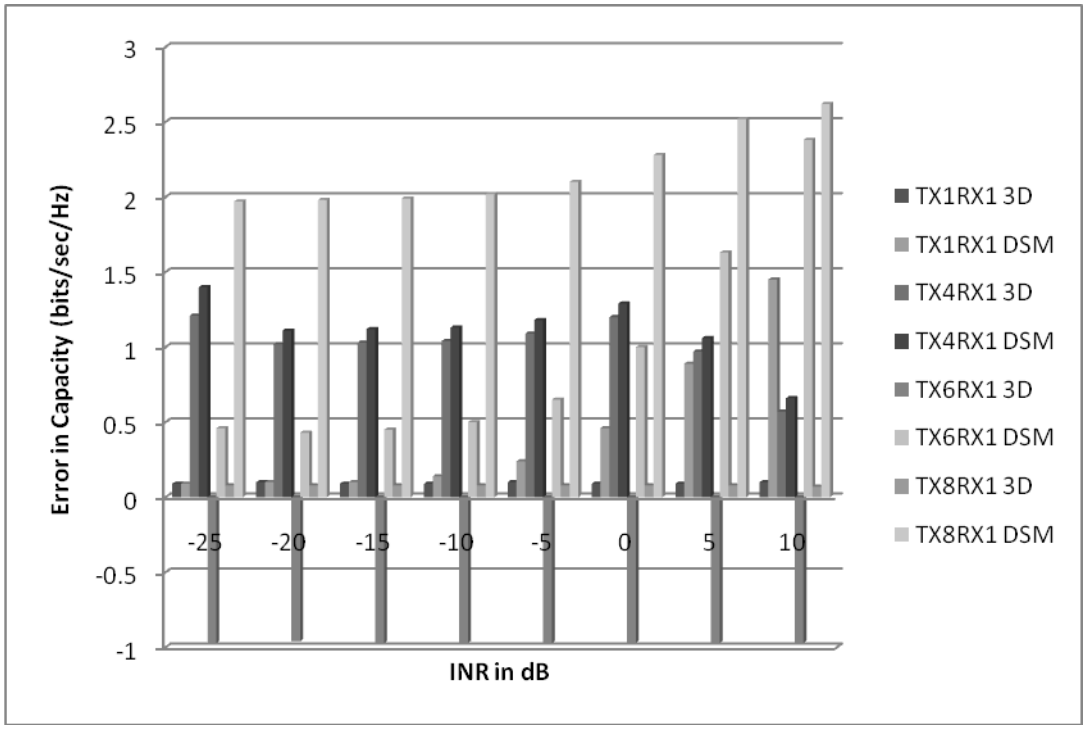

Figure **Error! No text of specified style in document.**.6: MEB tunnel error in capacities between the measurements and 3D ray-tracing model (3D), and measurements and Detailed signal model (DSM) with multi-antenna interferer located at Tx7 in figure 1. Four transmitter locations Tx1, Tx4, Tx6 and Tx8 were used for measurements.

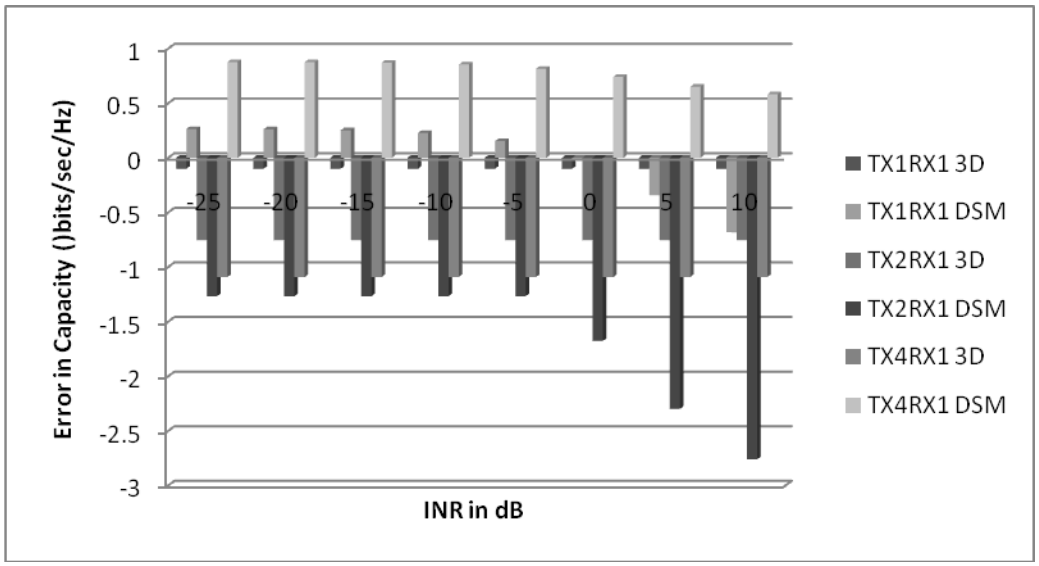

Figure **Error! No text of specified style in document.**.7: Park building tunnel error in capacities between the measurements and 3D ray-tracing model (3D), and measurements and Detailed signal model (DSM) with single antenna interferer located at Tx3 in figure 2. Three transmitter locations Tx1, Tx2, and Tx3 were used for measurements.

From these figures we observe that both the 3D ray-tracing model provides a capacity estimate of about 1 bit/sec/Hz for both the tunnels in the presence of interferers. The detailed signal model provides a capacity estimate of about 1 bit/sec/Hz except for transmitter location Tx8 in the MEB tunnel. The second interferer location Tx3 in the MEB tunnel has similar decrease in the capacity for both single and multi-antenna interference which shows that for small tunnels the location of the interference plays less of a role in capacity reduction than the INR. Figure 5.9 shows the effect of varying INR for a fixed SNR of 20 dB using 4 co-channel interferers with various spacing between the receiver antennas. Two matching techniques – self match and simultaneous conjugate match -- have been used at the receiver. The capacity decreases non-linearly with the increase in INR. This non-linear variation is due to the logarithmic variation of capacity in (21). At lower INR the capacity is maximized, the noise dominates, and the interference has less effect on the system. Below -25dB the INR can be neglected in this channel. At very high INRs the capacity is low. From Figure 5.9 we also observe that the simultaneous conjugate match provides the best capacity at small spacing regardless of the INR value.

UU IR Author Manuscript

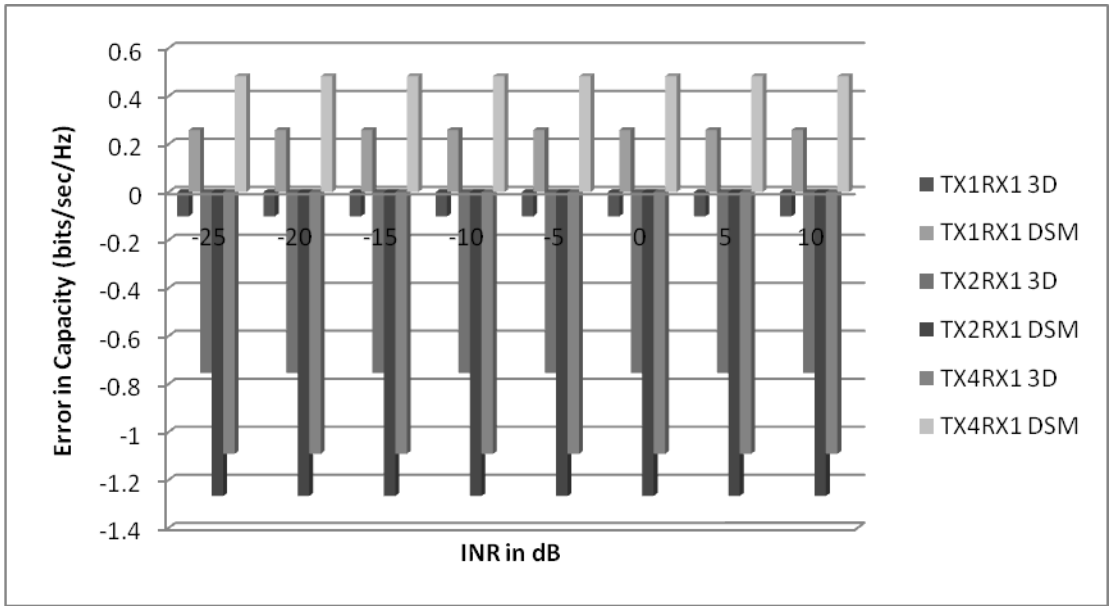

Figure **Error! No text of specified style in document.**.8: Park Tunnel error in capacities between the measurements and 3D ray-tracing model (3D), and measurements and Detailed signal model (DSM) with multi-antenna interferer located at Tx3 in figure 2. Three transmitter locations Tx1, Tx2, and Tx3 were used for measurements.

1.7 Conclusion

This paper provides a detailed signal model based on network theory to predict the multi-antenna capacity in the presence of co-channel interference. This model expands on previous channel models by including the simultaneous effects of co- and adjacent channel interference, antenna matching, efficiency, directivity and polarization. For both single and multi-antenna interference the results obtained from the detailed signal model and the 3D ray-tracing model are compared to those obtained from measurements in tunnels. We observe that for the MEB tunnel the modeled capacity using the detailed model is in the range of 1-2 bits/sec/Hz error except for location Rx3 where the capacity is within 3 bits/sec/Hz. The 3D ray-tracing method provides the capacity within 1 bit/sec/Hz in most locations except for Tx8 where the difference is about 2 bits/sec/Hz. For the Park building tunnel capacity obtained by using both the

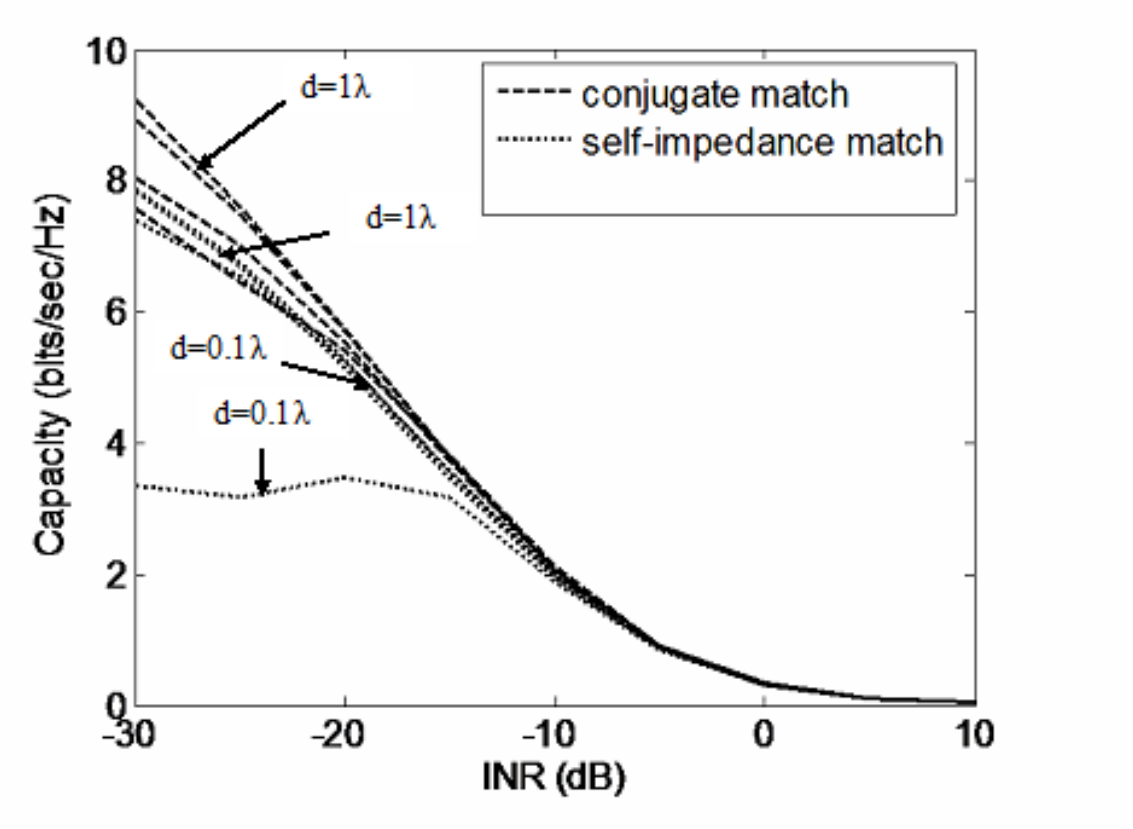

Figure **Error! No text of specified style in document.**.9. Capacity plotted as a function of INR for self match and simultaneous conjugate match at the receiver for a 2 X 2 MIMO system with varying spacing (0.1λ, 0.25λ, 0.5λ, 1λ). The SNR is set at 20 dB and the INR is varied from – 30 dB to 30 dB.

detailed signal model as well as the 3D ray-tracing model is within 1 bit/sec/Hz of the measured capacity. In the presence of interference for the MEB tunnel we observe that the 3D ray-tracing method provides capacity within 1.2 bits/sec/Hz and the detailed signal model provides capacity within 2 bits/sec/Hz to the measured capacity. For the Park tunnel with interference we observe that the 3D ray-tracing method provides capacity within 1 bits/sec/Hz and the detailed signal model provides capacity within 1.3 bits/sec/Hz to the measured capacity. The advantage of the 3D ray-tracing model is that although it needs information about the site under consideration it does not need

information about the Ricean K-factor which is an integral part of the detailed signal model. The detailed signal model does not need site specific information but does need information about the richness of multipath, the Ricean K-factor and separation distance between the transmitter and receiver. These results show that the multi-antenna performance can be well estimated by using the site-specific 3-D ray-tracing model and the detailed signal model. The antenna spacing plays an important role in capacity estimation of multi-antenna system. We observe that for small spacing the conjugate match provides higher capacity than the self match.

Acknowledgements

This work was partially supported by the National Science Foundation under grant #ECCS-0823927 and the Universal Research Corporation under a grant from the Air Force Research Laboratory. We would also like to thank our colleagues James Nagel and Jason Saberian for their time and help during the tunnel measurements.

References

[1] R. S. Blum," MIMO Capacity with Interference", IEEE Journal on Selected Areas in Communications, Vol. 21, NO. 5,pp. 793-801, JUNE 2003

[2] X.Yang, A.O.Petropulu, " Co-channel Interference Modeling and analysis in a Poisson field of interferers in wireless communications", IEEE Transactions on Signal Processing, Vol.51, No.1, January 2003

[3] Y.Song and S.D. Blostein, "MIMO Channel Capacity in Co-Channel Interference", in Proc, 21st Biennial Symposium on Communication, Kingston, Canada, Jan 2002,pp.220-224

[4] J. Koivunen, P. Almers, V.-M. Kolmonen, J. Salmi, A. Richter, F. Tufvesson, P. Suvikunnas, A. Molisch, and P. Vainikainen, "Dynamic multi-link indoor MIMO measurements at 5.3 GHz," in Proceedings of the 2nd European Conference on Antennas and Propagation (EuCAP 2007), Edinburgh, 2007

[5] D. Landon, C. Furse, "The MIMO Transmission Equation," IEEE Antennas and Propagation Symposium (APS), SanDiego, CA, July 7-11,2008

[6] C. Takahashi, **Z. Yun, M. F. Iskander**, G. Poilasne, V. Pathak, and J. Fabrega, "Propagation prediction and site planning software for wireless communication systems," IEEE Antennas and Propagation Magazine, vol. 49, no. 2, pp. 52-60, April 2007.

[7] Z. Yun, Z. Zhang, and M. F. Iskander, "A ray-tracing method based on the triangular grid approach and application to propagation prediction in urban environments," Proc IEEE Int. Symp. Information Theory (ISIT2004), vol. 50, pp. 750–758, May 2002.

[8] C. Takahashi, Z. Yun, M. F. Iskander, et al. "Propagation-Prediction and Site-Planning Software for Wireless Communication Systems" IEEE Antennas and Propagation Magazine, Vol. 49, No. 2, April 2007

[9] S. Y. Lim, Z. Yun, J. M. Baker, N. Celik, H.-S. Youn, and M. F. Iskander, "Radio propagation in stairwell: Measurement and simulation results," in IEEE Antennas and Propagation Society International Symposium, (Charleston, SC), June 2009

[10] M. L. Morris, M. A. Jensen, "Network model for MIMO system with coupled antennas and noisy amplifiers", IEEE Transactions on Antennas and Propagation, Vol 53, No.1,pp. 545-552, Jan 2005

[11] D. Palchak and B. Farhang-Boroujeny, "A software defined radio testbed for MIMO systems," in Proceedings of the SDR 06 Technical Conference and Product Exposition, (Orlando, FL), November 2006

[12] Claude Oestges and Bruno Clerckx, " MIMO Wireless Communication- From Real-World Propagation to Space-Time Code Design", Elsevier Ltd, 2007 ISBN: 9780123725356

[13] Peruvemba R. Sai A, Alyssa Magleby, James R. Nagel, and Cynthia Furse, "MIMO Wireless Communication for Aircraft Sensors," 12th Joint FAA/DOD/NASA Conference on Aging Aircraft, Kansas City Convention Center, May 04-07, 2009